Pure Appl. Chem., Vol. 75, No. 10, pp. 1371–1381, 2003.

Molecular structure and dynamics of proteins in solution: Insights derived from high-resolution NMR approaches*

Dennis A. Torchia‡ and Rieko Ishima

Molecular Structural Biology Unit, National Institute of Dental and Craniofacial Research, National Institutes of Health, Bethesda, MD 20892, USA

Abstract: This article reviews heteronuclear NMR techniques that are used to characterize the 3D structures and internal molecular dynamics of proteins in solution. Applications to several proteins that have been studied in our laboratory are presented. Topics discussed include sequential assignments, the use of nuclear Overhauser enhancement spectroscopy (NOESY) and residual dipolar coupling restraints to determine protein structure, and the use of relaxation measurements to obtain information about protein internal motions. Also discussed are recent computational approaches directed at increasing the efficiency of structure determination, as well as new methods for studying large proteins.

INTRODUCTION

The past decade has witnessed a phenomenal growth in the use of high-resolution NMR spectroscopy to obtain detailed information about the structure and dynamics of proteins, in order to elucidate their functions. Proteins are polypeptides composed of 20 types of monomer units, the naturally occurring amino acids. In order to function properly, the polypeptide chain must normally fold into a well-defined, compact structure. In general, nonpolar amino acid side chains pack into the hydrophobic interior, or core, of the molecule, while hydrophylic side chains make up the solvent-accessible protein surface. Although a folded protein is well ordered, significant portions of the protein are often flexible as well. Both well-ordered and flexible protein domains have roles in function.

The 3D structure of a protein is specified by the linear sequence of amino acids in the polypeptide chain. Despite progress in predicting the structure of a protein from its amino acid sequence [1], experimental methods remain the only reliable means to obtain high-resolution protein structures. The first protein structures were solved at high resolution over 40 years ago by X-ray diffraction. When single crystals of proteins are available, this method remains the most efficient means to obtain high-resolution structures of proteins. About 15 years ago, it was shown that solution structures of proteins having molecular weights below ca. 10 kDa could be solved [2] using 2D ^{1}H homonuclear NMR techniques [3]. The achievement made it possible, for the first time, to view protein structures in the absence of crystal contacts, and paved the way for NMR studies of larger proteins.

The study of larger proteins required the development of 2-4D heteronuclear NMR spectroscopy [4,5]. This approach was made feasible by recombinant DNA technology, which permitted efficient incorporation of ^{13}C, ^{15}N, and ^{2}H spins into proteins, and by advances in instrumentation. Herein, we review heteronuclear NMR techniques that are widely applied to study proteins in solution and also discuss approaches that are being developed to overcome limitations with current methodology.

---

*Plenary lecture presented at the IUPAC Polymer Conference on the Mission and Challenges of Polymer Science and Technology (IUPAC PC2002), Kyoto, Japan, 2–5 December 2002. Other presentations are published in this issue, pp. 1359–1402.

‡Corresponding author: E-mail: dtorchia@dir.nidcr.nih.gov

SEQUENTIAL SIGNAL ASSIGNMENTS

Typically, the first spectrum recorded of a protein of interest is a 2D ^{1}H-^{15}N HSQC spectrum. The HSQC spectrum of profilin, a 125-residue protein that regulates assembly of the cytoskeleton, is shown in Fig. 1a. The excellent signal dispersion indicates that profilin is a suitable candidate for a structure determination. However, in order to determine its structure, one must first assign nearly every ^{1}H, ^{15}N, and ^{13}C NMR signal frequency to a specific atomic site in each amino acid residue of the protein.

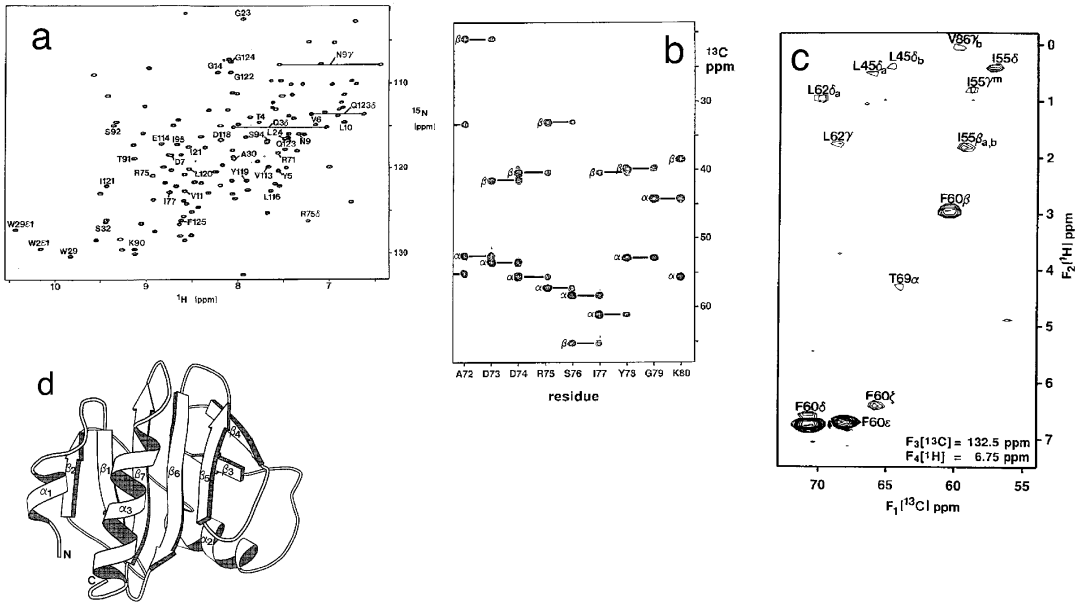

Fig. 1 Spectra and structure of profilin: (a) ^{1}H-^{15}N HSQC spectrum; (b) sequential strips from the 3D HNCACB spectrum; (c) one plane of the ^{1}H-^{13}C 4D NOESY spectrum; (d) average 3D solution structure.

Two 3D triple resonance experiments, termed HNCACB [6] and CBCA(CO)NH [7], efficiently provide signal assignments of protein backbone nuclei. Sequential strips, extracted from the HNCACB spectrum of profilin, are shown in Fig. 1b. Each strip shows up to four signals, two of which link the chemical shifts of an amide NH of each residue (identified at the bottom of Fig. 1b) to the chemical shifts of intraresidue Cα and Cβ spins, and two other signals that link the NH chemical shifts to those of the Cα and Cβ spins of the preceding residue. The interresidue and intraresidue linkages are distinguished by the CBCA(CO)NH spectrum (not shown), enabling one to align the data strips in sequential fashion. The identification of the amino acid types is made by using the chemical shifts of the Cα and Cβ signals, in conjunction with side chain chemical shifts obtained from additional 3D triple resonance experiments [8]. This information together with the known amino acid sequence provides the desired sequential signal assignments of profilin [9].

DETERMINATION OF THE 3D STRUCTURE OF A PROTEIN IN SOLUTION FROM NOESY-BASED DISTANCE RESTRAINTS

The sequential signal assignments, combined with measurements of secondary chemical shifts [10,11], and J-couplings [12,13], provide dihedral angle and hydrogen bond restraints that reliably identify regions of the polypeptide chain that adopt α-helical, β-strand, or coil-type conformations. However, these restraints are insufficient to determine the 3D structure of the protein. Rather, the crucial restraints needed to determine a protein structure in solution are approximate interproton distances derived from

cross-peaks observed in nuclear Overhauser enhancement spectroscopy (NOESY) spectra [14]. Fluctuating magnetic dipole–dipole interactions between pairs of protons are the source of NOESY cross-peaks. Although the dipolar interaction is a traceless second rank tensor that vanishes to first order in isotropic solution, it does not vanish in second order, and is the mechanism for proton cross-relaxation. A pair of protons that cross-relax exchange magnetization, resulting in a NOESY cross-peak that correlates their chemical shifts. Because NOESY cross-peak intensities are approximately proportional to r^{-6}, where r is the interproton distance, they rapidly decrease with r, and are observed only for proton pairs with r less than ca. 5 Å. Typically, cross-peak intensities are categorized as strong, medium, or weak, and assigned respective interproton distance restraints of less than ca. 2.7, 3.6, or 5.0 Å. Because of their approximate nature and short range, 1000 or more NOESY distance restraints are usually required to determine a protein structure. In addition, because of proton signal overlap, it is essential to obtain ^{15}N- and ^{13}C-separated 3D and 4D NOESY spectra [5], in order to maximize the number of unambiguous NOESY signal assignments. Over 10 unambiguous interproton distance restraints are obtained from one plane, Fig. 1c, of the 4D ^{13}C-separated NOESY spectrum of profilin. A ribbon diagram of the average structure of profilin, determined primarily from NOESY distance restraints using the X-PLOR protocol [15], is shown in Fig. 1d [16]. A crystal structure of profilin, determined subsequently [17], is in close agreement with the NMR structure.

RESIDUAL DIPOLAR COUPLINGS PROVIDE LONG-RANGE RESTRAINTS FOR STRUCTURE DETERMINATIONS

NOESY-based methodology has been used to determine over 1000 protein structures listed in the Protein Data Bank. However, because NOESY restraints are short range, it is difficult to determine the relative orientation of protein domains that are linked by a relatively small number of nuclear Overhauser effects (NOEs). This problem was apparent in the structure determination of ribosomal protein S4 Δ41, a protein that plays an important role in initiating ribosome assembly. The average NMR structure, Fig. 2a, reveals that the protein contains upper and lower domains. Although over 2000 NOESY restraints were used to determine the structure, only 12 interdomain NOEs were observed, and consequently the relative orientation of the 2 domains was not well defined [18]. This can be seen in Fig. 2b, which shows 9 NMR structures, which are superimposed, subject to the condition that the coordinate rmsd of the upper domain is minimized. While the ensemble of upper-domain structures closely superpose, the lower-domain structures do not. On the other hand, if the rmsd of the ensemble of lower-domain coordinates is minimized, the converse is observed. Therefore, the short-range NOESY distance restraints yield precise structures of the individual domains, but do not precisely define their relative orientation.

Long-range restraints were required to specify the relative orientation of the S4 Δ41 domains. Such restraints were obtained from measurements of residual dipolar couplings [19,20]. As noted above, the average dipolar interaction of two spins, such as an amide proton and its directly bonded ^{15}N, vanishes in isotropic solution. However, small, residual dipolar couplings are observed when an anisotropic medium is used to weakly align a protein [21]. In the case of S4 Δ41, liquid-crystalline media were used to slightly align the protein. Over 35 ^{1}H-^{15}N dipolar couplings were measured for each of the two domains of S4 Δ41 [22], and were used to determine the orientation of the residual dipolar coupling (alignment) tensor in each domain. Assuming that S4 Δ41 has a single conformation, the orientations of the two alignment tensors must be the same, when the two domains are correctly positioned. This condition restricts the relative orientation of the two domains. As seen in Fig. 2c, when residual dipolar couplings are included in the structure determination and NMR structures are again superposed to minimize the coordinate rmsd of the upper domain, the lower domain is restricted to a small range of orientations.

In the case of S4 Δ41, it was found [22] that the average orientation of the two domains in solution agreed with the orientation observed in an independently determined crystal structure. While sim-

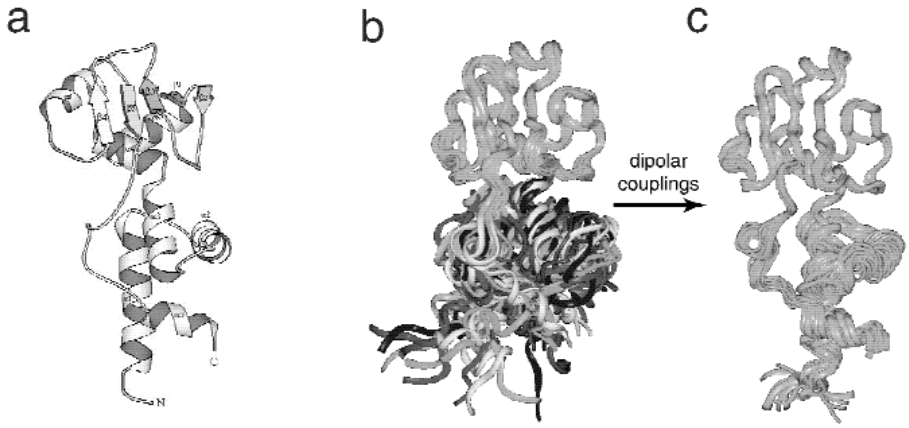

Fig. 2 Structure of S4 Δ41: (a) ribbon diagram of the average solution structure, depicting the folds of the upper and lower domains; (b) nine solution structures superimposed to minimize the rmsd of the coordinates of the upper domain, dipolar couplings not included; (c) same as b, but with residual dipolar couplings included in the structure determination.

ilar domain orientations have been observed for other proteins in solution and crystalline states, significant differences have also been noted [23]. Hence, it is important to determine the orientation of protein domains in solution, even when a crystal structure is available. This is particularly true when relatively few interdomain interactions stabilize a multidomain protein structure, making it more likely that a domain orientation could be altered by crystal contacts.

IMPROVING THE EFFICIENCY AND ACCURACY OF NOESY-BASED STRUCTURE DETERMINATIONS

The rate-limiting step in determining the NOESY-based 3D structures of profilin and S4 Δ41, and of proteins generally, is the laborious assignment of thousands of NOESY cross-peaks by hand. Recently, significant progress has been made in developing computer protocols that automate chemical shift [24], and NOESY signal assignments [25,26]. An important advantage of these latter programs is that they use the many ambiguous NOESY assignments, available at the initial stage of the structure determination, to generate an approximate protein fold. This initial fold is used to reduce the number of ambiguous NOESY assignments, and an improved structure is calculated. This process is repeated until essentially all NOEs are uniquely assigned and used to determine the final structure. The availability of such software is greatly accelerating the process of structure determination. In addition, the accuracy of any NOESY-based structure can be quickly tested by checking how well it predicts residual dipolar couplings [21].

PROTEIN DYNAMICS REVEALED BY SPIN RELAXATION MEASUREMENTS

Although structure determination is the goal of most protein NMR studies, it is widely appreciated that proteins are not rigid bodies, and that chemical bonds in proteins reorient as a consequence of internal motions. Such internal motions cause fluctuations in local fields at nuclei and are the source of nuclear spin relaxation. In proteins, magnetization of spin-1/2 nuclei (^{1}H, ^{13}C, and ^{15}N) relaxes via dipolar and anisotropic chemical shift mechanisms, whereas the spin-1 ^{2}H nucleus relaxes via the quadrupolar mechanism. For clarity, we now consider the case of dipolar relaxation of a ^{15}N nucleus by its directly attached proton, but note that similar remarks apply to the other relaxation mechanisms. Well-known expressions [5] show that the relaxation rate of ^{15}N longitudinal and transverse magnetization

($R_1 = 1/T_1$ and $R_2 = 1/T_2$ respectively) as well as the ^{15}N-{^1H} NOE are proportional to sums of spectral density functions, $J(\omega)$. The spectral density functions contain the information of interest about protein dynamics. When internal and overall motions of the protein are independent, and overall motion is isotropic, the model-free [27] expression for the spectral density function is

$$J(\omega) = S^2\tau_c/(1 + \omega^2\tau_c^2) + (1 - S^2)\tau/(1 + \omega^2\tau^2) \quad (1)$$

S^2 is the squared generalized order parameter, and contains information about the amplitude of internal motion ($S^2 = 0$ for isotropic internal motion of the NH bond axis, and $S^2 = 1$ when motion is absent), and $1/\tau = 1/\tau_c + 1/\tau_e$ where τ_c and τ_e are correlation times for overall and internal motions, respectively. R_1 and NOE values are determined solely by terms of the form $J(\omega_L)$, where ω_L is on the order of the Larmor frequency, while, in proteins, R_2 is dominated by zero frequency terms, $J(0)$. Examination of eq. 1 reveals that for those sites undergoing small amplitude internal motion, (i.e., S^2 ca. 1), the first term in eq. 1 dominates, and uniform relaxation rates, corresponding to overall motion alone, are observed. On the other hand, the relaxation rates of mobile sites vary and may differ significantly from those of rigid sites. In general, internal motions cause reductions in R_2 and NOE, relative to their rigid body values, whereas R_1 may increase or decrease, depending upon the details of the internal motion. More complex expressions for $J(\omega)$ have been developed to account for anisotropic overall motion and for two internal motions that take place on significantly different time scales [28]. Model-selection protocols are available to extract model-free parameters from measured relaxation rates [29,30].

Examination of eq. 1 reveals that the spectral density function reduces to its rigid body ($S^2 = 1$) form when $\tau_e >> \tau_c$, regardless of the actual value of S^2. This is a manifestation of the fact that dipolar, and all other second-rank tensor relaxation mechanisms, are insensitive to motions that are slower than the overall motion of the protein. However, slow internal motions on the ms–μs time scale, that modulate the isotropic (scalar) chemical shift, are a mechanism for transverse relaxation, termed herein conformational exchange. The exchange contribution, R_{ex}, to R_2 is most clearly revealed by measuring R_2 as a function of the RF field, B_{eff}, in the rotating reference frame. When conformational exchange is present, a plot of R_2 vs. B_{eff} exhibits a characteristic dispersion, from which R_{ex} can be obtained [31,32]. Measurements of R_{ex} as a function of B_{eff} and the static field [33] provide information about the correlation times and conformational states involved in the exchange process.

Finally, we note that residual dipolar couplings, unlike spin relaxation rates in solution, are sensitive to motions on the μs–ns time scale. Approaches are being developed to use dipolar couplings to elucidate dynamics on the μs–ns time scale [34].

RAPID INTERNAL DYNAMICS OF THE HIV PROTEASE

The HIV protease is a 22 kDa enzyme that is essential for function of the AIDS virus, and is a prime target for drugs directed against HIV. The crystal structure of the free HIV protease, Fig. 3a, was solved in 1989 [35], and subsequently hundreds of structures have been determined of the protein bound to various inhibitors and substrate mimics. Figure 3b reveals the structure of the bound protease, with inhibitor DMP323 bound at the active site [36]. At the base of the molecule, four β-strands, one coming from the N- and C-terminus of each monomer, make an anti-parallel β-sheet that stabilizes formation of the free active protease dimer. Comparison of Fig. 3a with Fig. 3b reveals that the only significant difference in the free and inhibitor-bound conformations of the protease occurs in the flaps, the pair of two-stranded β-sheets at the top of the molecule. Figure 3b shows that in the inhibitor-bound protease the flaps are fully closed over the inhibitor; whereas in the free protease, Fig. 3a, the flaps are semi-open. It is clear from Fig. 3b that the flaps must open to allow a ligand to emerge from the active site. Furthermore, the semi-open flap conformation of the free protease, Fig. 3a, does not allow substrates or inhibitors access to the empty active site. Therefore, the flaps must move to allow substrate to enter and product to exit the active site.

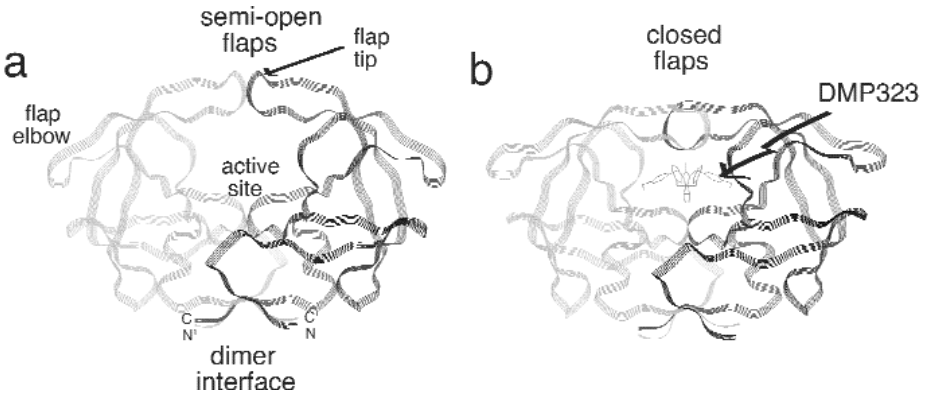

Fig. 3 Ribbon diagrams comparing the backbone organization of free and inhibitor-bound HIV protease: (a) free protease; (b) protease bound to DMP323, the latter displayed in a stick representation. The protease is a symmetric homodimer, and ribbons are shaded light and dark gray to distinguish the two monomers.

In order to characterize protease dynamics in solution, ^{15}N, T_1, T_2, and the ^{15}N-{^1H} NOE were measured for nearly every backbone amide site of the protease bound to DMP323 [37], and of the free protease [38]. Profiles of these parameters for the free protease, plotted vs. residue number in Figs. 4a–c, show rather uniform values for most amide sites, indicating little internal motion on the sub-ns time scale. However, the ^{15}N T_2 values and NOEs are, respectively, significantly larger and smaller than average for residues 38–41, 49–52, and 80. These residues are located in the β-hairpins at the tips of the flaps, a solvent exposed loop called the flap elbow, and a loop containing the conserved triad Pro79-Thr80-Pro81, respectively. The relaxation parameters observed for these residues suggest that they are flexible on the sub-ns time scale.

This conclusion is confirmed by the model-free parameters, S^2, and τ_e, derived from these measurements and plotted in Figs. 4d,e. Residues tentatively described as flexible in the previous paragraph have S^2 values significantly smaller than average and internal correlation times in the range of 0.1–1 ns. For example, residues 49–53 in the flap tips, all have S^2 values less than 0.75, and have an average S^2 of 0.62, nearly 40 % less than the average of residues not in the flaps. If one models the motion of the NH bond as diffusion in a cone, one finds the cone semiangle is 40° for $S^2 = 0.62$.

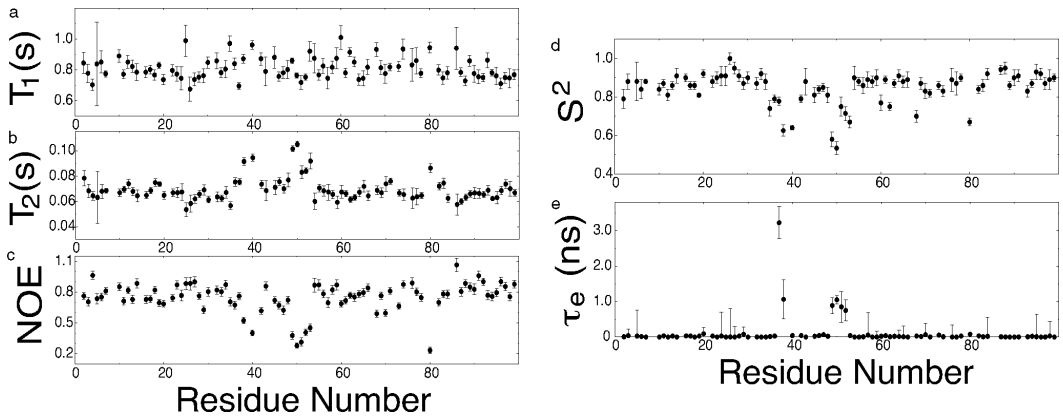

Fig. 4 Comparison of profiles of ^{15}N relaxation parameters (a–c) and model-free parameters (d,e) of free HIV protease at 20 °C: (a) T_1; (b) T_2; (c) NOE; (d) S^2; (e) τ_e; each parameter is plotted vs. residue number.

Residues 37–41 and 80 were also found to be flexible on the sub-ns time scale in the case of the protease/DMP323 complex in solution [37]. In addition, rotational diffusion coefficients characterizing the overall (rigid body) motion of the free and the inhibitor-bound proteases were essentially the same. However, in contrast to the results obtained for the free protease, the tips of the flaps were not flexible on the sub-ns time scale when the protease was bound to DMP323 [37]. These results are consistent with observations made in the crystalline state [35]. While crystal structures of the free protease reveal flap conformations that are static, the flap conformations vary among semi-open and closed forms, whereas, whenever the protease binds an inhibitor, the flaps are invariably closed and contribute to a hydrogen bond network that stabilizes the protease-inhibitor complex.

FLEXIBILITY OF THE TERMINAL DIMER INTERFACE OF THE PROTEASE

The structural heterogeneity of the flaps observed in protease crystal structures suggested that the flaps would be flexible in solution. However, the well-ordered interfacial β-sheet made by the four N- and C-terminal strands, that is observed in all crystal structures, gave no hint of flexibility. It was, therefore, surprising that residues in this β-sheet exhibited exchange contributions to R_2 [39,40]. These observations [39,40], have been confirmed by recent measurements of amide ^{1}H and ^{15}N R_2 dispersion profiles of the protease bound to DMP323, Figs. 5a–d, which provide strong evidence for motions on the ms–μs timescale in the dimer interface. The free protease R_2 dispersion profiles have shapes similar to those shown in Fig. 5; however, the dispersion amplitude of the free protease is 3–10-fold smaller than for the bound protease. The greater amplitude of the R_2 dispersion observed for the bound protease

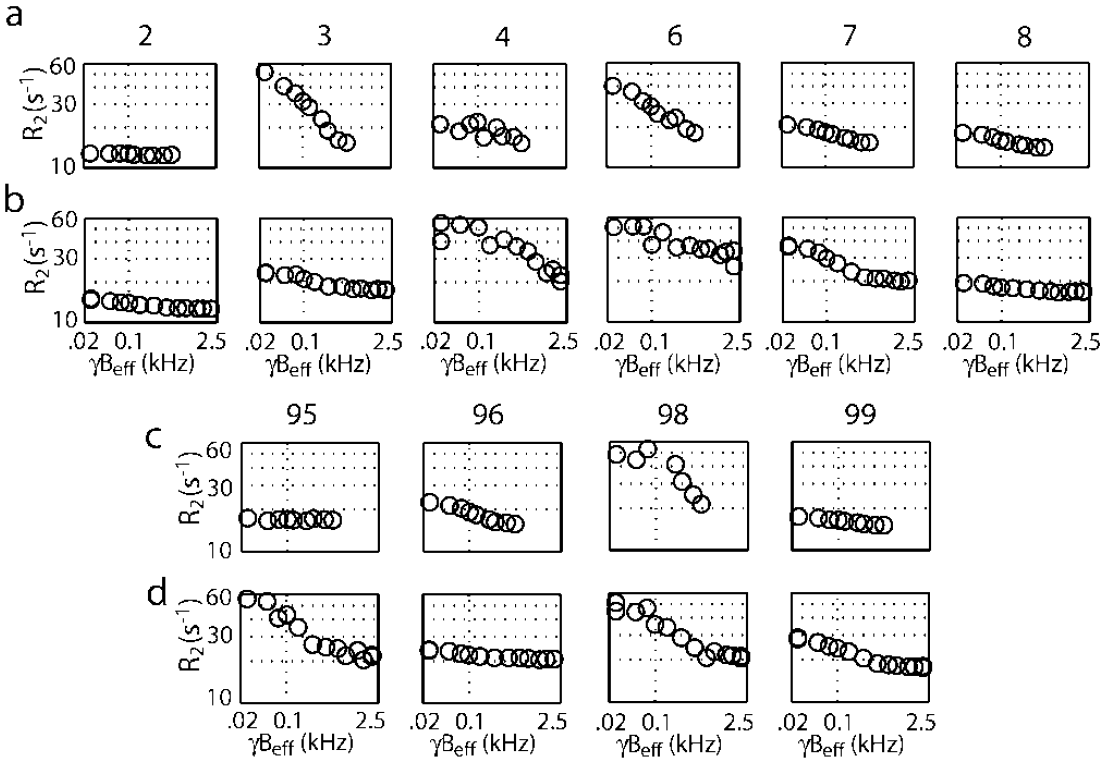

Fig. 5 ^{1}H and ^{15}N R_2 dispersion profiles observed for N- and C-terminal residues of HIV protease bound to DMP323: (a) ^{15}N, residues 2–8, (b) ^{1}H, residues 2–8; (c) ^{15}N, residues 95–99; (d) ^{1}H, residues 95–99. All data recorded on 500 MHz spectrometers.

is consistent with a study of protease terminal deletion mutants [41], which showed that DMP323 forms a complex with the protease dimer even in the absence of an intact terminal β-sheet.

The flexibility of the dimer interface has been related to protease processing reactions [39,40]. The protease precursor contains polypeptide chains that extend from both the N- and C-terminal residues of the mature protein. The protease cleaves these polypeptide extensions, and the Leu5-Trp6 peptide bond of the mature protein. These reactions require that a terminal strand of the protease insert into its active site, which requires that the strand separate from the terminal β-sheet. The flexibility observed for residues in the dimer interface by solution-state NMR indicates that such a structural fluctuation is plausible. Recently, conformational heterogeneity in the four-stranded sheet has been reported in the X-ray structure of the protease bound to a high affinity inhibitor [42], corroborating the conclusions regarding dimer interface flexibility derived from the NMR studies

Flexibility on the ms–μs time scale was also observed for the flaps of the free protease and the protease bound to DMP323. We refer the reader to the literature [38,43] for a discussion of these observations and their interpretation.

DYNAMICS OF METHYL SIDE CHAINS IN FREE AND BOUND PROTEASE

Studies of internal dynamics of proteins are not limited to the protein backbone. The relaxation of spins located in most aliphatic side chain sites can be measured by incorporating ^{2}H and/or ^{13}C into the protein [40,44–46]. Methyl sites are particularly attractive because their rapid three-fold rotation enhances sensitivity by decreasing T_1 while increasing T_2. The analysis of ^{2}H R_1 and R_2 values is straightforward [44], because the quadrupolar inteaction is the sole relaxation mechanism and R_{ex} is negligible. On the other hand, because ^{13}C relaxation is sensitive to conformational exchange, ^{13}C R_2 measurements can identify methyl sites undergoing slow motions [40].

Analysis of methyl ^{2}H and ^{13}C R_1 and R_2 values yielded similar values of S^2_{axis} (the order parameter of the C-C_{methyl} axis) for free and DMP323-bound protease [47]. The only exceptions to this statement are flap residues 50 and 54, which have $S^2_{axis} < 0.5$ only in the free protease. Numerous methyl sites are flexible, having $S^2_{axis} < 0.75$, and the most flexible sites, those having S^2_{axis} less than 0.5, are shown in Fig. 6a. In both free and bound protease, R_2 values of residues 3, 5, and 97 were RF field-dependent, implying that these residues experienced conformational exchange [47]. The methyl groups of these residues are in the hydrophobic interior of the terminal dimer interface, Fig. 6b. In agreement with the $^{1}H/^{15}N$ R_2 data described in the previous section, the RF field dependence was more pronounced for protease bound to DMP323 than for the free protein.

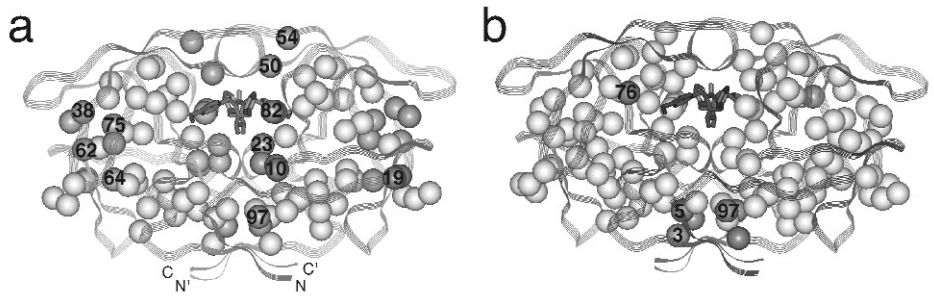

Fig. 6 Flexible methyl sites in HIV protease, where methyl carbon sites are depicted as spheres on the ribbon structures [36], of the protease-DMP323 complex: (a) numbered sites have significant motions on the sub-ns time scale, $S^2_{axis} < 0.5$; (b) numbered sites undergo conformational exchange on the ms–μs time scale. For clarity, only one of each pair of symmetry-related methyl carbons is numbered according to its position in the amino acid sequence. Note that $S^2_{axis} < 0.5$ for residues 50 and 54 only in the free protease.

It is interesting that the hydrophobic protease interior consists almost entirely of methyl-containing side chains, and nearly two-thirds of the amino acids that mutate in response to drugs contain methyl groups. Many of these sites are flexible [47], and their flexibility may allow the protease to fine-tune its structure by mutations that specifically impair binding to drugs.

RECENT ADVANCES IN NMR STUDIES OF LARGE PROTEINS

NMR applications have typically involved proteins with molecular weights less than 30 kDa; however, most proteins have higher molecular weights, and many interact with target molecules to form functional complexes that are larger still. For this reason, there is great interest in extending the size limit of NMR [48]. The principal factor limiting studies of large proteins is the rapid decay of transverse magnetization during the magnetization transfer steps in heteronuclear NMR experiments. This problem increases with the size of the protein, because R_2 is proportional to the overall correlation time. One approach that reduces R_2 combines deuteration of all CH sites, except the methyls of Leu, Val, and Ile, with uniform $^{15}N/^{13}C$ labeling [48]. Although deuteration reduced the number of observable NOEs, a 3D structure of maltose binding protein, MBP, which contains 370 amino acids, was obtained [48]. Augmenting the NOESY data with residual dipolar couplings yielded a higher-resolution structure of loaded MBP, which revealed that domain orientations in solution differed from those observed in the crystalline state [48].

High-quality data have been obtained for larger systems by combining $^{2}H/^{13}C/^{15}N$ labeling with TROSY selection of the slowly relaxing component of amide NH magnetization. Structures of two membrane proteins in micelles, systems having molecular weights of 50–60 kDa, have been solved at low resolution [49,50]. In addition, complete backbone assignments and secondary structures, of a 110 kDa homooctameric protein [51] and an 80 kDa single-chain protein [52], MSG, have been reported. Recently, the CRIPT-TROSY approach has been used to record HSQC spectra of the protein GroES in a chaperonin complex [53], with total molecular weight of 900 kDa.

Signal assignments of large proteins open the way to study their molecular dynamics. ^{15}N T_1 and T_2 values measured for MSG [52], showed that the protein tumbles isotropically in solution with a correlation time of 36 ns at 37 °C, and that several mobile loops observed in solution correspond to regions of the protein that are disordered in the crystal.

REFERENCES

1. A. G. Murzin. *Nature Struct. Biology* **8**, 110–112 (2001).
2. K. Wüthrich. *NMR of Proteins and Nucleic Acids*, Wiley, New York (1986).
3. R. R. Ernst, G. Bodenhausen, A. Wokaun. *Principles of Nuclear Magnetic Resonance in One and Two Dimensions*, Clarendon Press, Oxford (1987).
4. M. Ikura, L. E. Kay, A. Bax. *Biochemistry* **29**, 4659–4667 (1990).
5. J. Cavanagh, W. J. Fairbrother, A. G. Palmer, N. J. Skelton. *Protein NMR Spectroscopy: Principles and Practice*, Academic Press, San Diego (1996).
6. M. Wittekind and L. Mueller. *J. Magn. Reson. B* **101**, 201–205 (1993).
7. S. Grzesiek and A. Bax. *J. Am. Chem. Soc.* **114**, 6291–6293 (1992).
8. S. Grzesiek, J. Anglister, A. Bax. *J. Magn. Reson.* **101**, 114–119 (1993).
9. S. J. Archer, V. K. Vinson, T. D. Pollard, D. A. Torchia. *Biochemistry* **32**, 6680–6687 (1993).
10. D. S. Wishart and B. D. Sykes. *J. Biomol. NMR* **4**, 171–180 (1994).
11. G. Cornilescu, F. Delaglio, A. Bax. *J. Biomol. NMR* **13**, 289–302 (1999).
12. F. Cordier and S. Grzesiek. *J. Am. Chem. Soc.* **121**, 1601–1602 (1999).
13. A. Bax, G. W. Vuister, S. Grzesiek, F. Delaglio, A. C. Wang, R. Tschudin, G. Zhu. *Methods Enzymol.* **239**, 79–105 (1994).
14. K. Wüthrich. *Science* **243**, 45–50 (1989).

15. A. T. Brünger. *X-PLOR Manual Version 3.1: A System for X-RAY Crystallography and NMR*, Yale University, New Haven, CT (1992).
16. V. K. Vinson, S. J. Archer, E. E. Lattman, T. D. Pollard, D. A. Torchia. *J. Cell Biol.* **122**, 1277–1283 (1993).
17. A. A. Fedorov, K. A. Magnus, M. H. Graupe, E. E. Lattman, T. D. Pollard, S. C. Almo. *Proc. Natl. Acad. Sci. USA* **91**, 8636–8640 (1994).
18. M. A. Markus, R. B. Gerstner, D. E. Draper, D. A. Torchia. *EMBO J.* **17**, 4559–4571 (1998).
19. J. R. Tolman, J. M. Flanagan, M. A. Kennedy, J. H. Prestegard. *Proc. Natl. Acad. Sci. USA* **92**, 9279–9283 (1995).
20. N. Tjandra and A. Bax. *Science* **278**, 1111–1114 (1997).
21. A. Bax, G. Kontaxis, N. Tjandra. *Methods Enzymol.* **339B**, 127–174 (2001).
22. M. A. Markus, R. B. Gerstner, D. E. Draper, D. A. Torchia. *J. Mol. Biol.* **292**, 375–387 (1999).
23. V. Kanelis, J. D. Forman-Kay, L. E. Kay. *IUBMB Life* **52**, 291–302 (2001).
24. H. N. B. Moseley, D. Monleon, G. T. Montelione. *Methods Enzymol.* **339B**, 91–108 (2001).
25. T. Herrmann, P. Guntert, K. Wüthrich. *J. Mol. Biol.* **319**, 209–227 (2002).
26. J. P. Linge, S. I. O'Donoghue, M. Nilges. *Methods Enzymol.* **339B**, 71–90 (2001).
27. G. Lipari and A. Szabo. *J. Am. Chem. Soc.* **104**, 4546–4559 (1982).
28. A. G. Palmer. *Curr. Opin. Struct. Biol.* **7**, 732–737 (1997).
29. N. A. Farrow, R. Muhandiram, A. U. Singer, S. M. Pascal, C. M. Kay, G. Gish, S. W. Shoelson, T. Pawson, J. D. Forman-Kay, L. E. Kay. *Biochemistry* **33**, 5984–6003 (1994).
30. A. M. Mandel, M. Akke, A. G. Palmer. *J. Mol. Biol.* **246**, 144–163 (1995).
31. F. A. A. Mulder, N. R. Skrynnikov, B. Hon, F. W. Dahlquist, L. E. Kay. *J. Am. Chem. Soc.* **123**, 967–975 (2001).
32. J. P. Loria, M. Rance, A. G. Palmer. *J. Am. Chem. Soc.* **121**, 2331–2332 (1999).
33. O. Millet, J. P. Loria, C. D. Kroenke, M. Pons, A. G. Palmer. *J. Am. Chem. Soc.* **122**, 2867–2877 (2000).
34. J. Meiler, J. J. Prompers, W. Peti, C. Griesinger, R. Bruschweiler. *J. Am. Chem. Soc.* **123**, 6098–6107 (2001).
35. A. Wlodawer and J. W. Erickson. *Annu. Rev. Biochem.* **62**, 543–585 (1993).
36. P. Ala, R. J. DeLoskey, E. E. Huston, P. K. Jadhav, P. Y. S. Lam, C. J. Eyermann, C. N. Hodge, M. C. Schadt, F. A. Lewandowski, P. C. Weber, D. D. McCabe, L. J. Duke, C.-H. Chang. *J. Biol. Chem.* **273**, 12325–12331 (1998).
37. L. K. Nicholson, T. Yamazaki, D. A. Torchia, S. Grzesiek, A. Bax, J. D. Kaufman, S. J. Stahl, P. T. Wingfield, P. Y. S. Lam, P. K. Jadhav, C. N. Hodge, P. J. Domaille, C.-H. Chang. *Nature Struct. Biol.* **2**, 274–280 (1995).
38. D. I. Freedberg, R. Ishima, J. Jacob, Y. X. Wang, I. Kustanovich, J. M. Louis, D. A. Torchia. *Protein Sci.* **11**, 221–232 (2002).
39. R. Ishima, P. T. Wingfield, S. J. Stahl, J. D. Kaufman, D. A. Torchia. *J. Am. Chem. Soc.* **120**, 10534–10542 (1998).
40. R. Ishima, J. M. Louis, D. A. Torchia. *J. Am. Chem. Soc.* **121**, 11589–11590 (1999).
41. R. Ishima, R. Ghirlando, J. Tozser, A. M. Gronenborn, D. A. Torchia, J. M. Louis. *J. Biol. Chem.* **276**, 49110–49116 (2001).
42. K. K. Reiling, N. F. Endres, D. S. Dauber, C. S. Craik, R. M. Stroud. *Biochemistry* **41**, 4582–4594 (2002).
43. R. Ishima, D. I. Freedberg, Y. X. Wang, J. M. Louis, D. A. Torchia. *Structure* **7**, 1047–1055 (1999).
44. D. R. Muhandiram, T. Yamazaki, B. D. Sykes, L. E. Kay. *J. Am. Chem. Soc.* **117**, 11536–11544 (1995).
45. D. M. LeMaster and D. M. Kushlan. *J. Am. Chem. Soc.* **118**, 9255–9264 (1996).
46. A. L. Lee, J. L. Urbauer, A. J. Wand. *J. Biomol. NMR* **9**, 437–440 (1997).

47. R. Ishima, J. M. Louis, D. A. Torchia. *J. Mol. Biol.* **305**, 515–521 (2001).
48. L. E. Kay. *Methods Enzymol.* **339B**, 174–203 (2001).
49. A. Arora, F. Abildgaard, J. H. Bushweller, L. K. Tamm. *Nature Struct. Biol.* **8**, 334–338 (2001).
50. C. Fernandez, K. Adeishvili, K. Wüthrich. *Proc. Natl. Acad. Sci. USA* **98**, 2358–2363 (2001).
51. M. Salzmann, K. Pervushin, G. Wider, H. Senn, K. Wüthrich. *J. Am. Chem. Soc.* **122**, 7543–7548 (2000).
52. V. Tugarinov, R. Muhandiram, A. Ayed, L. E. Kay. *J. Am. Chem. Soc.* **124**, 10025–10035 (2002).
53. J. Fiaux, E. B. Bertelsen, A. L. Horwich, K. Wüthrich. *Nature* **418**, 207–211 (2002).